

Architecture and evaluation protocol for transformer-based visual object tracking in UAV applications

Augustin Borne* ^{1,2,3}, Pierre Notin ^{1,2}, Dr. Christophe Hennequin ¹, Dr. Sebastien Changey ¹, Dr. Stephane Bazeille ², Prof. Christophe Cudel ², and Prof. Franz Quint ³

¹French-German Research Institute of Saint-Louis, Saint-Louis, France

²Université de Haute-Alsace, Mulhouse, France

³Karlsruhe University of Applied Sciences, Karlsruhe, Germany

Abstract

Object tracking from Unmanned Aerial Vehicles (UAVs) is challenged by platform dynamics, camera motion, and limited onboard resources. Existing visual trackers either lack robustness in complex scenarios or are too computationally demanding for real-time embedded use. We propose an Modular Asynchronous Tracking Architecture (MATA) that combines a transformer-based tracker with an Extended Kalman Filter, integrating ego-motion compensation from sparse optical flow and an object trajectory model. We further introduce a hardware-independent, embedded oriented evaluation protocol and a new metric called Normalized time to Failure (NT2F) to quantify how long a tracker can sustain a tracking sequence without external help. Experiments on UAV benchmarks, including an augmented UAV123 dataset with synthetic occlusions, show consistent improvements in Success and NT2F metrics across multiple tracking processing frequency. A ROS 2 implementation on a Nvidia Jetson AGX Orin confirms that the evaluation protocol more closely matches real-time performance on embedded systems.

Keywords: UAV tracking, visual object tracking, vision transformers, estimation filter, motion compensation, embedded systems, real time

1 Introduction

Tracking objects from an Unmanned Aerial Vehicle (UAV) is difficult due to high platform dynamics, frequent object occlusions, and significant camera motion. Moreover, the entire perception pipeline must run in real time on Size, Weight, and Power (SWaP) constrained embedded hardware. At the same time, reliable onboard tracking is essential for many UAV applications.

Visual Object Tracking (VOT) aims to localize a target in a video sequence from an initial position. The search is usually restricted to a local region for computational efficiency. However, this approach struggles with fast motion, occlusions, and camera movement. Early tracking

models relied on correlation filters, e.g. MOSSE [1] and KCF [2]. While computationally efficient, they are sensitive to occlusions and large deformations. The advent of deep learning introduced Siamese network-based trackers, e.g. SiamFC [3] and SiamRPN [4]. They significantly improved accuracy by learning robust appearance representations, yet they can struggle with long-term occlusions and significant scale changes. More recently, transformer-based architectures have been adapted for VOT, modeling global context and improving resilience to difficult challenges such as occlusions, deformations, and background clutter, but are computationally heavy. Notable models include TransT [5], OSTrack [6], and SeqTrack [7]. Recent approaches also explore prompt-based and foundation model trackers, leveraging textual or visual prompts to enable flexible tracking, including PIVOT [8] or ChatTracker [9], however prompt-based models are often too large for embedded real-time deployment. These limitations highlight that there is still substantial room for improvement in designing tracking solutions that are both accurate and lightweight for real-time UAV applications. Despite progress in VOT, key challenges remain. Standard trackers often ignore the temporal dimension, and struggle with rapid target motion, occlusions, or camera-induced movement. Accuracy and efficiency trade-offs are significant: transformers are precise but slow, correlation filters are fast but less accurate, and Siamese networks lie in between. Moreover, standard evaluation protocols assume a single tracker, while embedded or robotic systems may involve multiple blocks at different frequencies, making real-time performance highly dependent on both algorithm and hardware.

In this study, we address these challenges by proposing a Modular Asynchronous Tracking Architecture (MATA), which combines a transformer-based tracker, MixFormerV2 [10], with an Extended Kalman Filter (EKF) [11]. This design leverages the high accuracy of vision transformers while benefiting from the EKF's real-time estimation capabilities on embedded devices. The EKF integrates camera ego-motion compensation, estimated via a lightweight sparse Lucas-Kanade optical flow [12], with a constant-velocity object trajectory

*Corresponding author: augustin.borne@uha.fr

model, improving robustness under occlusions and rapid target motion. To evaluate multi-module tracking systems independently of hardware constraints, we introduce a hardware-independent evaluation protocol that simulates an onboard processing chain. It models asynchronous data flows between modules, allowing each component to operate at its own frequency. This modular protocol enables fair cross-platform comparison while assessing both temporal robustness and real-time feasibility. We also formalize the Normalize time to failure (NT2F) metric, which quantifies how long a tracker can maintain a target, and introduce an augmentation tool that synthetically generates smooth occlusions of varying shapes and sizes following target trajectories, to better evaluate trackers under occlusion scenarios. This tool was used to create an augmented version of UAV123 (UAV123+occ). The evaluation protocol is validated by comparing its results to a ROS 2 implementation on a Nvidia Jetson AGX Orin [13]. We validate the MATA method on UAV123 [14], VTUAV [15], and UAV123+occ dataset. The key contributions of this work are:

1. A hardware-independent evaluation protocol simulating asynchronous multi-block processing
2. A Modular Asynchronous Tracking Architecture (MATA) that enhances robustness in difficult conditions, including occlusions.
3. The design of a robustness metric and an augmentation tool to generate synthetic occlusions, enabling systematic evaluation of tracker performance under challenging scenarios.

2 MATA: a Modular Asynchronous Tracking Architecture

We propose a tracking framework called the Modular Asynchronous Tracking Architecture (MATA), which organizes independent, interchangeable blocks around a transformer-based tracking algorithm. In an image sequence, an object’s apparent motion comes from two sources: the object’s own movement and the motion of the camera. MATA models these two effects separately and combine them in an estimation-filter block to produce bounding boxes at real-time rates. As shown in figure 1, the architecture includes four main modules: a camera-motion compensation block that estimates the camera’s ego-motion, a visual tracking block based on a vision-transformer model, and an object-motion estimation block that fuses the previous outputs with a dynamic model to generate high-frequency bounding-box predictions. Thanks to its modular design, any block in MATA can be replaced, upgraded, removed, or extended with additional components as needed.

2.1 Explainable scoring mechanism

VOT models can estimate prediction confidence in various ways, from direct score prediction to metrics based

on response maps or feature distributions. For instance, MixFormerV2 [10] confidence is estimated by an MLP on special tokens, while OTrack [6] uses the maximum value in the center heatmap. Both integrate confidence estimation end-to-end, but deep networks may produce overconfident scores that poorly reflect true tracking accuracy, reducing reliability for downstream tasks and making uncertainty harder to interpret. A confidence score representing a probability within $[0, 1]$ is better for interpretability. Applying a softmax to a neural network’s outputs naturally enforces this range and normalization. Based on this principle, we propose a confidence score that leverages the probability mass functions (PMFs) produced by MixFormerV2 model for each bounding box coordinate across the discrete spatial positions of the feature map. The bounding box is defined by its top-left and bottom right corners coordinates noted respectively (x_{tl}, y_{tl}) and (x_{br}, y_{br}) . Let $X_{x_{tl}}, X_{y_{tl}}, X_{x_{br}}$ and $X_{y_{br}}$ be discrete random variables. Their PMFs are defined as $p_i(x) = \mathbb{P}(X_i = x)$ with $i \in \{x_{tl}, y_{tl}, x_{br}, y_{br}\}$ and $x \in [0, N]$ where N is the number of features in the PMF. For each PMF, the peak position is defined as $k_i^* = \arg \max_k p_i(k)$.

$$S_i = \sum_{k=k_{\min,i}}^{k_{\max,i}} p_i(k) \quad (1)$$

$$k_{\min,i} = \min\left(k_i^* - \frac{\alpha N}{2}, 1\right)$$

$$k_{\max,i} = \max\left(k_i^* + \frac{\alpha N}{2}, N\right)$$

For each coordinate i , we compute a score S_i as defined in Eq. 1. A window of width αN , where α is a hyperparameter (set to 0.03 in our experiments), centered at k_i^* , is defined. The score for each coordinate is computed as the sum of probabilities within this window. The bounds $k_{\min,i}$ and $k_{\max,i}$ define the window limits and handle boundary effects at the edges of the feature map. The final confidence score is defined by the lowest confidence score over the four coordinate scores, $S = \min_i S_i$. By utilizing these PMFs, this scoring method quantifies how concentrated the predicted probabilities are around their modes, providing an interpretable and spatially grounded confidence estimate for the bounding box localization. While the score is applied in 1D along each bounding box coordinate due to the special 1D output format of MixFormerV2, it can be easily extended to 2D heatmaps by replacing the linear window around the mode with a square window over the spatial grid, provided the heatmap resolution is sufficient.

2.2 Camera movement compensation

Camera ego-motion compensation removes the apparent motion caused by the camera rather than by the target, which is essential for isolating true object dynamics. Ego-motion can be estimated using Visual-inertial fusion or directly from images. To the best of our knowledge, no dataset in the literature provides sufficient calibrated IMU–image tracking data from a UAV perspective. Thus, we rely on image-based methods only. Cam-

era motion is approximated with geometric models of varying complexity [16], ranging from translation and similarity transforms to affine and full projective homographies. A practical and lightweight solution, used in OpenCV [17], tracks sparse features detected with standard corner or keypoint detectors [18, 19] using pyramidal Lucas–Kanade optical flow [20], and estimates an affine transform between frames. Each frame is then warped accordingly, with slight cropping or zooming to hide border artifacts.

In our application setting, onboard computation is severely constrained, making feature-based estimation impractical because feature detection and matching dominate runtime. To estimate inter-frame camera motion, we use a two-stage approach combining sparse optical flow and homography optimization. Unlike affine models, the homography is better suited to the large view-point variations typical of low-altitude UAV imagery. To reduce computational cost, we sample points on a regular grid rather than performing feature detection. We then use the classical approach with the pyramidal Lucas–Kanade algorithm to track point, producing correspondences $\{(\mathbf{p}_i, \mathbf{p}'_i)\}_{i=1}^N$, where \mathbf{p}_i and \mathbf{p}'_i respectively denote the positions of the i -th point in the current and next frame. Outliers are removed with RANSAC [21], retaining only inliers for transformation estimation. To better capture UAV camera motion, which can include significant perspective changes at low altitude, we model the 2D inter-frame relationship using an homography $\mathbf{H} \in \mathbb{R}^{3 \times 3}$, with g the homography projection as detailed in equation 2.

$$g(x, y) = \begin{bmatrix} x' \\ y' \\ 1 \end{bmatrix} \text{ with } s \begin{bmatrix} x' \\ y' \\ 1 \end{bmatrix} \sim H \begin{bmatrix} x \\ y \\ 1 \end{bmatrix} \quad (2)$$

$$H = \begin{bmatrix} h_{11} & h_{12} & h_{13} \\ h_{21} & h_{22} & h_{23} \\ h_{31} & h_{32} & h_{33} \end{bmatrix}$$

We compute the covariance of the estimated homography using the first-order approximation of non-linear parameter uncertainty, as described in Hartley and Zisser-

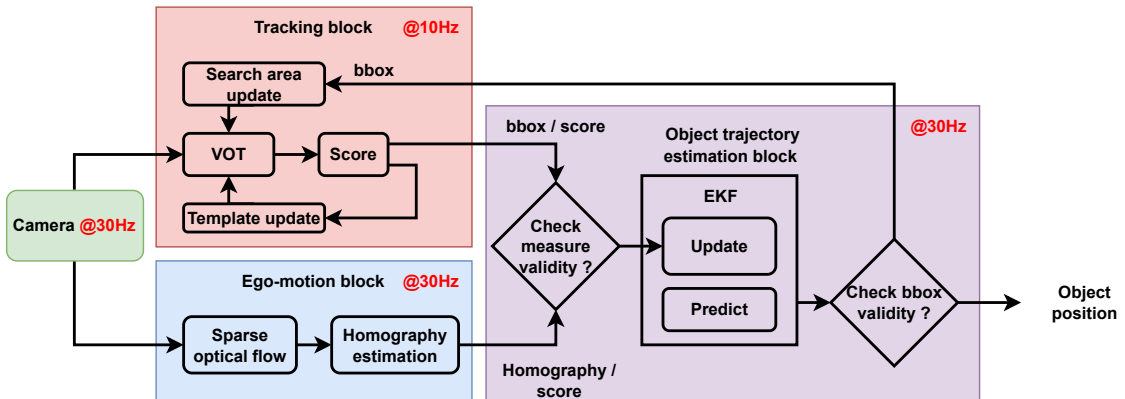
man [22], Result 5.10. This covariance matrix quantifies the uncertainty in the estimated transformation and is used as a confidence score for the estimated inter-frame ego-motion in downstream tasks.

2.3 Object trajectory estimation

The objective is to estimate the true trajectory of the object across time, ensuring a consistent representation of its motion in the 2D image frame. This estimation is non-trivial because the observed 2D motion results from the combination of two distinct dynamic components: the ego-motion of the camera and the intrinsic motion of the object. This is typically handled using estimation filters, most notably Kalman filter (KF) based [23] approaches. In VOT field, KF have been employed to enhance base trackers, providing higher robustness to occlusion such as mean-shift [24, 25] and STC [26], while in multi-object tracking, variants like SORT [27] improve tracking by combining a KF with efficient data association. The BOT-SORT variant [28] incorporates ego-motion compensation to enhance tracking performance, while OC-SORT [29] introduces an Observation-Centric Re-Update (ORU) mechanism that uses virtual trajectories to stabilize updates after extended periods of prediction-only tracking. The estimation filter yields estimations when the tracker cannot provide a reliable position either while it is unavailable due to computing time, or because the object becomes unobservable (e.g., due to occlusion), requiring the position to be predicted from camera motion estimation and target dynamic model.

For our estimation filter, we employ an Extended Kalman Filter (EKF) [30] to handle the inherent nonlinearity of the observed system. This serves as a proof of concept demonstrating that combining an estimation filter with a vision-transformer-based VOT model can improve tracking performance. For the object’s intrinsic motion, a constant-velocity model is adopted, providing a simple yet effective dynamic representation for short time periods without the complexity of more sophisticated models including acceleration, jerk or turn rate dynamics. Camera ego-motion is modeled using an homog-

Figure 1: Overview of the Modular Asynchronous Tracking Architecture: Example with tracker running at 10 Hz, estimation filter at 30 Hz and ego motion at 30 Hz.



raphy transformation as described in section 2.2. The filter state and measurements vectors are defined in equation 3. The state vector is combining the bounding box ¹ coordinates $\mathbf{X}_{tl} = [x_{tl}, y_{tl}]$, $\mathbf{X}_{br} = [x_{br}, y_{br}]$, the homography parameters $\mathbf{X}_H = [h_{11}, h_{12}, \dots, h_{32}, h_{33}]$, and the bounding box center velocity $\mathbf{X}_v = [\dot{x}_c, \dot{y}_c]$. The measurement vector follows the same partitioning and is composed only of the observable quantities $\mathbf{Z}_{tl} = [x_{tl}, y_{tl}]$, $\mathbf{Z}_{br} = [x_{br}, y_{br}]$ and $\mathbf{Z}_H = [h_{11}, h_{12}, \dots, h_{32}, h_{33}]$. Since no direct measurements of the bounding box center velocity are available, \mathbf{X}_v are estimated through the prediction step of the filter.

$$\begin{aligned} \mathbf{X} &= [\mathbf{X}_{tl} \ \mathbf{X}_{br} \ \mathbf{X}_H \ \mathbf{X}_v]^\top \\ \mathbf{Z} &= [\mathbf{Z}_{tl} \ \mathbf{Z}_{br} \ \mathbf{Z}_H]^\top \end{aligned} \quad (3)$$

During prediction, the predicted state vector is computed from the state transition function f that can be split in four parts similarly to state vector \mathbf{X} , giving the equations 4. Considering g the homography projection as defined in 2.2 based on the homography matrix derived from the coefficients of estimated states $\mathbf{X}_{H,k-1}$, and $\mathbf{J}_g(x, y)$ the Jacobian of g with reference to pixel coordinates (x, y)

$$\begin{aligned} \mathbf{X}_k &= f(\mathbf{X}_{k-1}) = \begin{bmatrix} \mathbf{X}_{tl,k} \\ \mathbf{X}_{br,k} \\ \mathbf{X}_{H,k} \\ \mathbf{X}_{v,k} \end{bmatrix} \\ \begin{bmatrix} \mathbf{X}_{tl,k} \\ \mathbf{X}_{br,k} \\ \mathbf{X}_{H,k} \\ \mathbf{X}_{v,k} \end{bmatrix} &= \begin{bmatrix} \mathbf{p}(\mathbf{X}_{tl,k-1}) + \mathbf{J}_g(\mathbf{X}_{v,k-1})dt \\ \mathbf{p}(\mathbf{X}_{br,k-1}) + \mathbf{J}_g(\mathbf{X}_{v,k-1})dt \\ \mathbf{X}_{H,k-1} \\ \mathbf{J}_g(\mathbf{X}_{v,k-1}) \end{bmatrix} \end{aligned} \quad (4)$$

For each processed frame, the tracker and ego-motion components provide a measurement along with a confidence score. Since both components rely on image data, their outputs are highly dependent on scene conditions and can be significantly variable. The confidence score reflects, to some extent, the reliability of each measurement. We therefore introduce a rejection mechanism prior to the EKF, ensuring that only high-confidence measurements are incorporated into the filter. As a consequence, the measurement noise covariance matrix \mathbf{R} is set with fixed low values, reflecting the assumed reliability of the retained measurements. However, this strategy remains sensitive to false positives, which may still degrade the EKF estimation quality.

The EKF initial state \mathbf{X}_0 is set as the initialization bounding box for \mathbf{X}_{bb_0} , with homography \mathbf{X}_{H_0} set to the identity and bounding box velocity \mathbf{X}_{v_0} set to zero. The process noise covariance \mathbf{Q} and the initial state covariance \mathbf{P}_0 are treated as hyper-parameters and have been tuned experimentally, with different values assigned to the bounding box, ego-motion, and velocity components to balance responsiveness and stability.

¹A bounding box is defined by its top-left (tl) and bottom-right (br) corners.

2.4 Overall MATA system

The proposed system (*cf.* figure 1) adopts a multi-block architecture, integrating camera-ego compensation, a tracker, and an estimation filter to provide robust, real-time visual object tracking on UAV platforms. The first block, the camera-ego compensation module, takes each input image and estimates the apparent motion induced by the UAV's own movement (*cf.* section 2.2). It outputs the inter-frame transformation along with the associated covariance. The second block, the tracker, receives the input image and outputs the target bounding box along with a confidence score. Depending on the underlying VOT algorithm, it may use fixed, online, or hybrid templates. In our approach, we make minimal modifications, when possible, the original confidence measure is replaced with the score described in section 2.1, and any template update mechanism is simplified to a threshold-based update τ_{template} . The third block, the estimation filter, fuses information from the tracker and the camera-ego compensation module as seen in section 2.3. The filter performs partial updates whenever new measurements arrive, as the tracker and camera-ego compensation modules operate at different frequencies. It produces a refined estimate of the target bounding box, providing a more robust and temporally consistent tracking result. The blocks are interconnected as follows. To update the tracker, we maintain an exponentially weighted moving average (EWMA) of the predicted confidence score. If the EWMA falls below a threshold τ_{ewma} or the current score drops significantly relative to the EWMA (by more than τ_{diff}), the tracker measurement is discarded; otherwise, it is used to update the target state. The inter-frame transformations from the ego-motion block are used only if their covariance is below a maximum threshold τ_σ . The tracker search region is updated based on the refined bounding box provided by the estimation filter. This system faces several challenges, including handling measurements at varying frequencies with computational delays, running in parallel on resource-constrained embedded platforms, and designing an evaluation protocol that accounts for these real-time and asynchronous characteristics.

3 Experiment

3.1 Embedded oriented evaluation protocol

Most tracking benchmarks, such as the VOT challenges [31], provide several protocols to evaluate accuracy, robustness, and real-time performance. In the short-term protocol, the tracker is reinitialized after each failure, thus focusing on accuracy in nominal conditions. The long-term protocol (LTP), dominant in the literature, initializes once and evaluates continuous localization and target-presence confidence. To account for real-time constraints, VOT2021 [32] introduced a real-time short-term variant in which frames are processed at a fixed rate (e.g., 20 FPS), and missing predictions are com-

pleted using a zero-order hold. This protocol jointly evaluates tracking accuracy and inference speed, thereby reflecting real-time tracking performance as a function of the underlying hardware. Consequently, when sufficient computational resources are available such that all frames are processed in real time, this protocol becomes equivalent to the long-term evaluation protocol. One intuitive option is to evaluate trackers by applying down-sampling to the input frames, which yields what we refer to as the down-sampling evaluation protocol (DSP). In this protocol, frames are uniformly sub-sampled (e.g., keeping every n th frame), resulting in sequences with lower effective frame rate. Such sub-sampling has been used in evaluation studies to investigate tracker performance at different temporal resolutions by discarding intermediate frames [33]. While DSP is easy to implement and represents a step toward assessing frame rate effects, it remains insufficient for real-time evaluation, as simply down-sampling the input does not take into account the actual processing time of the tracker. Furthermore, all these protocols assume a monolithic tracker that directly processes image frames, which is unrealistic for embedded or robotic systems. In practice, a full processing pipeline consists of multiple interconnected modules each operating at its own frequency. Real-time behavior then depends not only on algorithmic complexity but also on the hardware platform, meaning that the same tracker can behave very differently on a GPU powered system versus a lighter embedded device. To bridge the gap between development, benchmarking, and deployment, we propose an embedded oriented evaluation protocol (EOP) that mimics an onboard processing chain. It evaluates tracking using independent blocks with different update rates and optional one-period latency to simulate block processing time (e.g., a 5 Hz tracker on a 30 Hz stream processes every sixth frame and outputs one step later). Blocks communicate via a shared structure, with missed updates being either propagated or skipped according to each block rules. The frequency and output delay of each block are fully tunable by hand and act as hyper-parameters, independent of hardware or software. This allows replicating the same processing conditions across different platforms and implementations. By design, it is modular, enabling new components to be added easily.

We can see in Fig. 2 that three evaluation protocols are presented: LTP, DSP, and the proposed EOP protocol. In this example, the target tracker processes one out of every four frames (approximately 7.5 Hz), and we aim to obtain an overall estimate of the performance it would achieve on an embedded system. In the LTP timeline, the tracker processes every frame; as a result, the predictions closely match the ground truth. However, this scenario is unrealistic, as it does not account for computational delays. The second approach, based on downsampling the dataset (DSP), increases the motion between frames, but in practice remains similar to LTP: the tracker still processes every frame without delay, and additional information is lost due to discarded frames. In contrast, in the EOP timeline, the processing delay is explicitly taken into account. A zero-order hold is applied to the

prediction until a new output is produced by the VOT block. Consequently, this evaluation more closely reflects the actual behavior of a tracker running on an embedded system. Finally, Fig. 2 also allows a comparison between classical VOT algorithms (EOP timeline) and the proposed MATA tracking algorithms. Thanks to the asynchrony of its constituent blocks, MATA is able to generate a new prediction at every frame, thereby mitigating the computational delay inherent to the VOT model.

3.2 Datasets

To ensure a representative evaluation under aerial tracking conditions, we focus on datasets specifically designed for UAV-based visual object tracking. In particular, we use the UAV123 dataset [34], a widely adopted benchmark for aerial tracking performance, and the VTUAV dataset [35], considering only the RGB part of its test split. Although these datasets provide valuable evaluation material, they contain few sequences with occlusion², even though UAV tracking often encounters partial or complete occlusions from vegetation, buildings, or environmental obstacles. These scenarios are crucial for evaluating trajectory estimation filters.

To address this limitation and better evaluate the robustness of MTA, we developed a data augmentation tool to generate artificial occlusions. For each frame, a binary occlusion mask is generated based on hand-crafted features such as shape, motion, and timing, specifying the start and end frames of the occlusion event. From these, the system samples start and end positions outside the image and generates a small set of “hit points” where the occlusion should intersect the target ground truth. A per-frame trajectory is then obtained by linear interpolation between these points, with small random acceleration jitter added to mimic natural motion. For each occlusion event, a single occlusion object is first selected from several geometric shapes, including rectangles (*cf.* Fig. 3c), ellipses, circles (*cf.* Fig. 3a), blobs, or irregular polygons (*cf.* Fig. 3b) and its shape parameters are randomly sampled and scaled to the target size. This same object is then used throughout the entire sequence, moving along the per-frame trajectory to produce the occlusion. At each frame of the occlusion event, the binary mask of the shape is alpha-blended onto the RGB frame, producing smooth occlusions. Importantly, only the overall shape and the start/end frames of each occlusion event are hand-crafted. All other parameters, including alpha, size, exact shape parameters, number of intersection points, speed, and acceleration, are randomly sampled, ensuring that the augmented sequences are non-deterministic, which prevents any bias in the evaluation. For fair comparison between algorithms, the random seed was fixed so that each method is evaluated on the same sequence of augmented occlusion scenarios. Ground-truth annotations are left unchanged, forcing the tracker and filter to rely on motion prediction during these intervals.

²Respectively $\approx 12\%$ and $\approx 20\%$ of number of sequences for VTUAV and UAV123

Figure 2: Comparison of evaluation protocols: the long-term protocol (LTP) commonly used in the literature; the down-sampling protocol (DSP), which ignores processing delays; and the proposed asynchronous frame processing (EOP) protocol, which accounts for processing delays. Example of a VOT tracker running at 7.5–10 Hz, effectively processing every fourth frame. Differences in prediction rate can be observed between a classical VOT tracker (see EOP timeline) and the proposed MATA architecture.

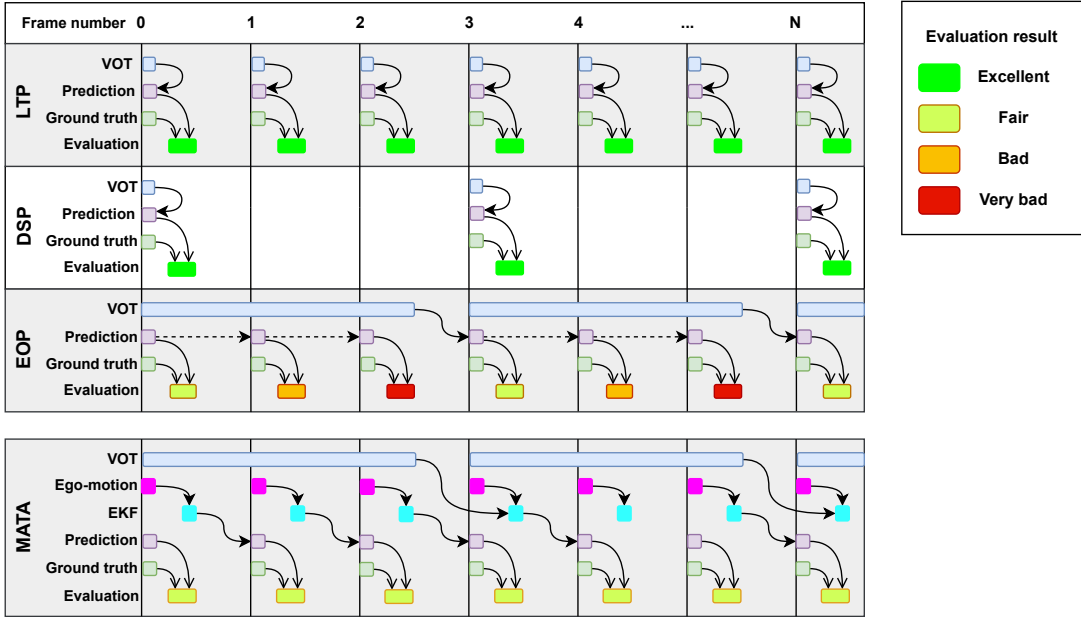


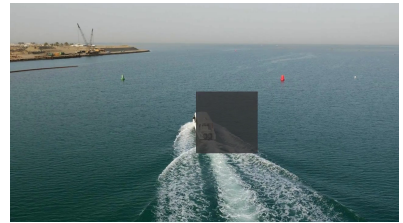
Figure 3: Example of shape applied to sequences on UAV123 dataset



(a) Circle shape



(b) Polygon and stripe shape



(c) Rectangle shape

3.3 Evaluation metrics

To evaluate the performance of each algorithm, we adopt standard evaluation metrics commonly used in the VOT community. We are using precision rate, the distance between predicted and ground-truth centers, and success rate (SR), the fraction of frames with sufficient bounding-box overlap. The MSR captures success across various overlap thresholds. We are using a normalized precision rate (PR) to account for varying object sizes and resolutions. Computational efficiency is reported via frames per second (FPS). The definitions and computation protocols for these metrics follow those presented in [36]. However, these classical metrics fail to capture how long a tracker can maintain a reliable tracking before a failure occurs. This limitation becomes particularly evident in scenarios where the tracker has no influence on the camera motion, for instance, when the camera continues to follow the object even after the tracker has lost it. In such cases, a tracker might “recover” the target purely by chance, which artificially inflates its performance.

To better quantify temporal persistence, several works have proposed time-linked robustness measures, such as

the Mean Time Between Failures (MTBF) [37], the tracking length [38], or the robustness metric used in the VOT challenges. These metrics estimate how often a tracker fails or how long it remains on target across entire sequences. Inspired by these approaches but aiming for a simpler and more interpretable measure, we introduce the Normalized Time-to-Failure (NT2F) which quantify how long a tracker maintain a valid target estimate before the first failure, normalized by the sequence length. Given a sequence of N frames, let IoU_t denote the intersection-over-union between the predicted and ground-truth bounding boxes at frame t , and let τ be a failure threshold (we use $\tau = 0$). For each sequence, the frame index of the first failure T_f is computed and the sequence $NT2F$ score is obtained with equation 5.

$$NT2F = \frac{T_f}{N}$$

$$T_f = \begin{cases} \min\{t \in [0, N - 1] \mid \text{IoU}_t \leq \tau\}, & \text{if exists,} \\ N, & \text{otherwise} \end{cases} \quad (5)$$

At the dataset level, the $NT2F$ metric is computed as the

mean of the individual $NT2F$ sequence values. This metric measures the portion of a sequence during which the tracker keeps the target before losing it for the first time. $NT2F$ is a normalized variant of the tracking length metric, focusing on how long a tracker can reliably track without external help.

3.4 Experimental setup

The system is evaluated on high-performance server and embedded edge platforms. Server experiments use an NVIDIA A100 GPU with both standard and proposed evaluation protocols (*cf.* section 3.1). In this study We employ six modular blocks: simulated camera (30 Hz), optical flow (30 Hz), VOT tracker (various frequency), motion filter 2.3 (30 Hz), decision (30 Hz), and saving modules (30 Hz). With the exception of the tracker block, all modules operate in real time on SWaP hardware, so the one-period delay is applied exclusively to the tracker. We vary the tracking frequency to characterize the system under different possible embedded configurations. We simulate tracking at speed from 5 to 30 FPS with the filter fixed at 30 FPS. After experimental trials, we observed the best results when using an ego-motion block based on a 16×16 matrix of points, uniformly distributed over the image. The method is validated on an NVIDIA Jetson AGX Orin representative of edge-AI platforms. For the embedded evaluation, the system is implemented within a ROS 2 framework, with each component running in a separate node inside its own Docker container. We allocate at least one CPU core per container, and two cores for the filter and tracker, which leverage a multithreaded executor to parallelize subscriber callbacks and computation. Communication uses the default DDS implementation. The experiment assesses system behavior under 50 W power mode. We evaluate two transformer-based state-of-the-art trackers, OTrack [6] and MixFormerV2 [10]. These models achieve competitive accuracy on literature tracking benchmarks. For the evaluation, UAV123 provides per-frame annotations, whereas VTUAV provides annotations only every 10th frame. Therefore, to compute the metrics, we subsample the predictions for the VTUAV evaluation, while using all predicted states for UAV123.

4 Results

Table 1 compares baseline trackers and their MATA variants on three datasets using long-term evaluation protocol and the proposed evaluation protocol (EOP). MATA consistently improves $NT2F$ for both trackers across all datasets. For OTrack, it also increases SR. For MixFormerV2 it slightly reduces SR except for EOP at 10Hz, but yields notable $NT2F$ gains. Overall, MATA primarily enhances long-term robustness while maintaining competitive SR performance. We observe an overall metric reduction between EOP @ 30 Hz and EOP @ 10 Hz, this is show the impact of tracker speed on performance.

Table 2 reports results on UAV123+occ at 10 Hz across

different challenges. MATA improves both SR and $NT2F$ for OTrack in all categories, with notable gains under occlusion and high dynamics. For MixFormerV2, MATA also improves most challenges, with a slight drop only in the out-of-view case, while maintaining comparable or higher $NT2F$. Overall, MATA enhances robustness under challenging conditions. The ablation study was conducted on the UAV123+occ dataset (*cf.* section 3.2) using the proposed evaluation protocol, with all trackers operating at 15 Hz. Results are summarized in table 3. As shown in this study, MATA (Configuration 2) consistently outperforms baseline MixFormerV2 (Configuration 1), particularly in $NT2F$, demonstrating robust long-term tracking. Configuration 3 shows that the explainable score mainly benefits long-term stability, improving $NT2F$ while keeping PR and SR comparable to the baseline. Removing camera motion compensation (Configuration 4) leads to a clear performance drop, highlighting its importance for accurate motion prediction. Alternative dynamic models using acceleration and jerk terms (Configurations 5 and 6) partially recover this loss, but remain inferior to the final constant-velocity MATA model. Disabling measurement thresholding (Configuration 7) slightly degrades performance, confirming the benefit of filtering unreliable measurements. Overall, these results confirm that each component of the proposed MATA framework contributes to the final performance, with the estimation filter design and camera motion compensation being key factors for robust long-term tracking. Table 4 reports the performance of tested trackers on the NVIDIA Jetson Orin AGX using the UAV123+occ dataset. The EOP and LTP columns report the absolute differences of SR and $NT2F$ between server evaluations and embedded system results. EOP accounts for the tracker’s actual embedded speed, whereas LTP does not. We observe that the EOP protocol reproduces more closely the embedded performance than LTP, indicating that EOP better captures the effect of real-time and asynchronous processing on resource-constrained hardware. Interestingly, the MATA-enhanced architecture no longer provides clear improvements in the embedded setup, suggesting that its benefits may be diminished under actual hardware constraints (hypotheses for this are discussed in section 5).

5 Discussion

The results show that MATA enhances long-term robustness across diverse conditions, while the EOP protocol provides a more realistic assessment of embedded tracking performance under real-time constraints.

The experimental results confirm that EOP offers a closer approximation of embedded tracking performance than LTP. When tracker speed is correctly configured, EOP reproduces embedded trends well, making it a valuable tool for early-stage embedded system design. In contrast, LTP ignores real-time constraints and therefore overestimates achievable performance. Compared to UAV123, the relatively low variation in VTUAV perfor-

Table 1: Performance of OTrack and MixFormerV2, with and without MTA, on UAV123, UAV123+occ, and VTUAV under LTP and EOP protocols. EOP is evaluated at 30 Hz and 10 Hz, the latter matching the runtime observed on NVIDIA Jetson Orin.

Protocol	VOT	MATA	UAV123		UAV123+occ		VTUAV	
			SR	NT2F	SR	NT2F	SR	NT2F
LTP	OTrack	✗	82.8	79.5	75.9	72.7	74.2	59.3
	OTrack	✓	83.6	79.5	78.5	74.1	74.8	61.1
	MixFormerV2	✗	84.3	79.1	78.2	68.8	75.6	55.2
	MixformerV2	✓	83.2	79.7	77.2	72.0	73.9	59.0
EOP @ 30 Hz	OTrack	✗	80.1	76.9	73.3	70.1	74.9	59.4
	OTrack	✓	81.9	77.9	76.0	72.2	75.7	61.6
	MixFormerV2	✗	81.9	77.5	75.8	67.2	76.2	55.2
	MixformerV2	✓	79.1	78.6	74.5	73.0	74.9	60.4
EOP @ 10 Hz	OTrack	✗	63.9	56.2	57.9	50.9	72.8	55.8
	OTrack	✓	69.8	64.4	65.8	60.0	75.5	58.2
	MixFormerV2	✗	65.5	52.2	60.8	44.5	74.4	48.4
	MixformerV2	✓	68.5	64.2	64.7	60.3	72.6	56.4

Table 2: Metrics per challenges on UAV123+occ with EOP evaluation with tracker at 10Hz

VOT	MATA	Occlusion		Distractor		High dynamic		Out of view	
		SR	NT2F	SR	NT2F	SR	NT2F	SR	NT2F
OTrack	✗	50.2	43.4	67.8	60.6	32.0	16.1	41.2	39.8
OTrack	✓	59.9	49.9	74.6	65.0	38.3	24.0	47.1	35.9
MixFormerV2	✗	52.9	37.0	70.3	50.6	36.2	14.9	46.5	32.8
MixformerV2	✓	59.1	50.8	72.4	61.1	35.1	25.1	46.4	36.7

Table 3: Impact of individual components on tracking performance on UAV123+occ, with tracking at 10 Hz using EOP.

#	Ego motion	EKF	Score	Details	PR	SR	MSR	NT2F
1	✗	✗	✗	MixFormerV2 (Baseline)	79.3	60.8	51.8	44.5
2	✓	✓	✓	MATA (section 2.4)	78.1	64.7	53.5	60.3
3	✗	✗	✓	section 2.1	<u>78.8</u>	60.8	51.5	46.4
4	✗	✓	✓	no camera compensation	76.4	61.6	51.5	48.1
5	✓	✓	✓	constant acceleration model	77.9	<u>64.5</u>	<u>53.3</u>	57.0
6	✓	✓	✓	constant jerk model	75.4	62.4	51.6	54.9
7	✓	✓	✓	no threshold on measurements	77.5	63.1	52.5	<u>57.6</u>

mance across LTP, EOP @ 30 Hz, and EOP @ 10 Hz is likely due to sparse annotations. This sparsity leads to the loss of fine-grained ground-truth target states, especially important with SR where traditional trackers might recover the target and inflate the SR value. However, the performance degradation is more pronounced in term of NT2F. We also observe a remaining gap remains between EOP and embedded results. This discrepancy mainly arises from EOP’s assumption that computation latency dominates, whereas in ROS 2 systems, communication latency plays a significant role. Even real-time-capable modules, such as ego-motion estimation, may be slowed by inter-node communication. In practice, each

block is subject to three types of latency: processing delay (blocking), waiting delay (e.g., awaiting new input), and communication delay (non-blocking but cumulative). These latencies are highly variable and non-deterministic on embedded platforms, unlike the constant delays assumed in EOP.

MATA improves robustness over the baseline with some limitations. Under LTP, it increases NT2F while maintaining comparable SR, demonstrating improved long-term stability. Under EOP, its advantage grows as tracker speed decreases, confirming its effectiveness for low-FPS tracking and occlusion scenarios. However, MATA relies heavily on accurate ego-motion compensa-

Table 4: Embedded performance on UAV123+occ (Jetson Orin AGX). EOP and LTP show absolute differences of SR and NT2F with reference to the embedded baseline

VOT	MATA	Embedded			EOP			LTP		
		SR	NT2F	FPS	SR	NT2F	FPS	SR	NT2F	FPS
OTrack	✗	58.6	51.0	10.5	3.7	4	10.5	17.3	21.7	30
OTrack	✓	58.4	51.3	9.2	0.5	1.6	9.2	20.1	22.8	30
MixFormerV2	✗	63.8	51.0	11.1	5.7	8.5	11.1	14.4	17.8	30
MixFormerV2	✓	59.7	49.8	9.7	1.0	3.8	9.7	17.5	22.2	30

tion, as confirmed by the ablation study. The remaining performance gap between EOP and embedded evaluations highlights limitations of the current MATA implementation. Since MATA was tuned under EOP assumptions, delayed ego-motion estimates in the embedded system directly reduce its effectiveness, indicating a primarily engineering-related limitation. Moreover, the current MATA formulation assumes instantaneous measurements, which does not hold in current ROS 2 implementation. Future work will therefore focus on reducing communication latency and extending MATA to explicitly model and compensate for measurement delays.

Thus, these findings demonstrate that MATA significantly improves long-term robustness, while EOP effectively bridges the gap between algorithm design and realistic embedded deployment.

6 Conclusion

This paper addressed the conventional VOT limitations in UAV scenarios with the MATA framework, which integrates ego-motion compensation and estimation filter with modern deep trackers. The experiments on the UAV123 dataset augmented with synthetic occlusions demonstrated that MATA consistently improves long-term performance. The proposed embedded oriented evaluation protocol which aimed to mimics embedded implementation further highlighted the benefits of the proposed framework under realistic speed constraints. Future work will focus on improving confidence interpretability, extending the evaluation protocol with communication delay, and exploring more efficient embedded implementations.

Acknowledgments

This work is financed by the Agence de l’Innovation de Défense (AID) from the french ministry of defense.

References

- [1] D. S. Bolme, J. R. Beveridge, B. A. Draper, and Y. M. Lui, “Visual object tracking using adaptive correlation filters,” in *2010 IEEE Computer Society Conference on Computer Vision and Pattern Recognition*, pp. 2544–2550, 2010.
- [2] J. F. Henriques, R. Caseiro, P. Martins, and J. Batista, “High-speed tracking with kernelized correlation filters,” *IEEE Trans. Pattern Anal. Mach. Intell.*, vol. 37, p. 583–596, Mar. 2015.
- [3] L. Bertinetto, J. Valmadre, J. F. Henriques, A. Vedaldi, and P. H. S. Torr, “Fully-convolutional siamese networks for object tracking,” in *Computer Vision – ECCV 2016 Workshops* (G. Hua and H. Jégou, eds.), (Cham), pp. 850–865, Springer International Publishing, 2016.
- [4] B. Li, J. Yan, W. Wu, Z. Zhu, and X. Hu, “High performance visual tracking with siamese region proposal network,” in *2018 IEEE/CVF Conference on Computer Vision and Pattern Recognition*, pp. 8971–8980, 2018.
- [5] X. Chen, B. Yan, J. Zhu, D. Wang, X. Yang, and H. Lu, “Transformer tracking,” 2021.
- [6] B. Ye, H. Chang, B. Ma, S. Shan, and X. Chen, “Joint Feature Learning and Relation Modeling for Tracking: A One-Stream Framework,” in *Computer Vision – ECCV 2022: 17th European Conference, Tel Aviv, Israel, October 23–27, 2022, Proceedings, Part XXII*, (Berlin, Heidelberg), pp. 341–357, Springer-Verlag, Oct. 2022.
- [7] X. Chen, H. Peng, D. Wang, H. Lu, and H. Hu, “Seqtrack: Sequence to sequence learning for visual object tracking,” in *2023 IEEE/CVF Conference on Computer Vision and Pattern Recognition (CVPR)*, pp. 14572–14581, 2023.
- [8] S.-F. Chen, J.-C. Chen, I.-H. Jhuo, and Y.-Y. Lin, “Improving visual object tracking through visual prompting,” *IEEE Transactions on Multimedia*, vol. 27, pp. 2682–2694, 2025.
- [9] Y. Sun, F. Yu, S. Chen, Y. Zhang, J. Huang, Y. Li, C. Li, and C. Wang, “Chattracker: enhancing visual tracking performance via chatting with multimodal large language model,” in *Proceedings of the 38th International Conference on Neural Information Processing Systems, NIPS ’24*, (Red Hook, NY, USA), Curran Associates Inc., 2024.

- [10] Y. Cui, T. Song, G. Wu, and L. Wang, “Mixformerv2: efficient fully transformer tracking,” in *Proceedings of the 37th International Conference on Neural Information Processing Systems, NIPS ’23*, (Red Hook, NY, USA), Curran Associates Inc., 2023.
- [11] G. Welch and G. Bishop, “An introduction to the kalman filter,” tech. rep., University of North Carolina at Chapel Hill, USA, 1995.
- [12] B. D. Lucas and T. Kanade, “An iterative image registration technique with an application to stereo vision,” in *Proceedings of the 7th International Joint Conference on Artificial Intelligence - Volume 2, IJCAI’81*, (San Francisco, CA, USA), p. 674–679, Morgan Kaufmann Publishers Inc., 1981.
- [13] NVIDIA, “Nvidia announces availability of jetson agx orin developer kit to advance robotics and edge ai,” *NVIDIA Newsroom*, Mar 2022.
- [14] M. Mueller, N. Smith, and B. Ghanem, “A benchmark and simulator for uav tracking,” in *Computer Vision – ECCV 2016* (B. Leibe, J. Matas, N. Sebe, and M. Welling, eds.), (Cham), pp. 445–461, Springer International Publishing, 2016.
- [15] P. Zhang, J. Zhao, D. Wang, H. Lu, and X. Ruan, “Visible-thermal uav tracking: A large-scale benchmark and new baseline,” in *2022 IEEE/CVF Conference on Computer Vision and Pattern Recognition (CVPR)*, pp. 8876–8885, 2022.
- [16] R. Hartley and A. Zisserman, *Multiple View Geometry in Computer Vision*. Cambridge University Press, 2 ed., 2004.
- [17] G. Bradski, “The OpenCV Library,” *Dr. Dobb’s Journal of Software Tools*, 2000.
- [18] J. Shi and Tomasi, “Good features to track,” in *1994 Proceedings of IEEE Conference on Computer Vision and Pattern Recognition*, pp. 593–600, 1994.
- [19] E. Rublee, V. Rabaud, K. Konolige, and G. Bradski, “Orb: An efficient alternative to sift or surf,” in *2011 International Conference on Computer Vision*, pp. 2564–2571, 2011.
- [20] J.-Y. Bouguet, “Pyramidal implementation of the lucas kanade feature tracker description of the algorithm,” tech. rep., Intel Corporation, 1999.
- [21] M. A. Fischler and R. C. Bolles, “Random sample consensus: a paradigm for model fitting with applications to image analysis and automated cartography,” *Commun. ACM*, vol. 24, p. 381–395, June 1981.
- [22] R. Hartley and A. Zisserman, *Multiple view geometry in computer vision*. Cambridge: Cambridge Univ. Press, 2. edition, 17.printing ed., 2018.
- [23] R. E. Kalman, “A new approach to linear filtering and prediction problems,” *Journal of Basic Engineering*, vol. 82, pp. 35–45, 03 1960.
- [24] V. Karavasili, C. Nikou, and A. Likas, “Visual tracking by adaptive kalman filtering and mean shift,” in *Artificial Intelligence: Theories, Models and Applications* (S. Konstantopoulos, S. Perantonis, V. Karkaletsis, C. D. Spyropoulos, and G. Vouros, eds.), (Berlin, Heidelberg), pp. 153–162, Springer Berlin Heidelberg, 2010.
- [25] I. A. Iswanto and B. Li, “Visual object tracking based on mean-shift and particle-kalman filter,” *Procedia Computer Science*, vol. 116, pp. 587–595, 2017. Discovery and innovation of computer science technology in artificial intelligence era: The 2nd International Conference on Computer Science and Computational Intelligence (ICCSI 2017).
- [26] K. Mehmood, A. Jalil, A. Ali, B. Khan, M. Murad, W. U. Khan, and Y. He, “Context-aware and occlusion handling mechanism for online visual object tracking,” *Electronics*, vol. 10, no. 1, 2021.
- [27] A. Bewley, Z. Ge, L. Ott, F. Ramos, and B. Uppcroft, “Simple online and realtime tracking,” in *2016 IEEE International Conference on Image Processing (ICIP)*, IEEE, Sept. 2016.
- [28] N. Aharon, R. Orfaig, and B.-Z. Bobrovsky, “Bot-sort: Robust associations multi-pedestrian tracking,” 2022.
- [29] J. Cao, J. Pang, X. Weng, R. Khirodkar, and K. Kitani, “Observation-centric sort: Rethinking sort for robust multi-object tracking,” 2023.
- [30] A. E. Bryson, *Applied Optimal Control, Optimization, Estimation and Control*. New York: Routledge, 1st edition ed., 1975.
- [31] M. Kristan, J. Matas, A. Leonardis, T. Vojir, R. Pflugfelder, G. Fernandez, G. Nebehay, F. Porikli, and L. Čehovin, “A novel performance evaluation methodology for single-target trackers,” *IEEE Transactions on Pattern Analysis and Machine Intelligence*, vol. 38, pp. 2137–2155, Nov 2016.
- [32] M. Kristan, J. Matas, A. Leonardis, M. Felsberg, R. Pflugfelder, J.-K. Kaemarainen, H. J. Chang, M. Danelljan, L. C. Zajc, A. Lukežič, O. Drbohlav, J. Kaepylae, G. Haeger, S. Yan, J. Yang, Z. Zhang, G. Fernandez, M. Abdelpakey, G. Bhat, L. Cerkezci, H. Cevikalp, S. Chen, X. Chen, M. Cheng, Z. Cheng, Y.-C. Chiu, O. Cirakman, Y. Cui, K. Dai, M. M. Dasari, Q. Deng, X. Dong, D. K. Du, M. Dunnhofer, Z.-H. Feng, Z. Feng, Z. Fu, S. Ge, R. K. Gorthi, Y. Gu, B. Gunsell, Q. Guo, F. Gurkan, W. Han, Y. Huang, F. J. Lawin, S.-J. Jhang, R. Ji, C. Jiang, Y. Jiang, F. Juefei-Xu, Y. Jun, X. Ke, F. S. Khan, B. Hak Kim, J. Kittler, X. Lan, J. H. Lee, B. Leibe, H. Li, J. Li, X. Li, Y. Li, B. Liu, C. Liu, J. Liu,

- L. Liu, Q. Liu, H. Lu, W. Lu, J. Luiten, J. Ma, Z. Ma, N. Martinel, C. Mayer, A. Memarmoghadam, C. Micheloni, Y. Niu, D. Paudel, H. Peng, S. Qiu, A. Rajiv, M. Rana, A. Robinson, H. Saribas, L. Shao, M. Shehata, F. Shen, J. Shen, K. Simonato, X. Song, Z. Tang, R. Timofte, P. Torr, C.-Y. Tsai, B. Uzun, L. Van Gool, P. Voigtlaender, D. Wang, G. Wang, L. Wang, L. Wang, L. Wang, L. Wang, Y. Wang, Y. Wang, C. Wu, G. Wu, X.-J. Wu, F. Xie, T. Xu, X. Xu, W. Xue, B. Yan, W. Yang, X. Yang, Y. Ye, J. Yin, C. Zhang, C. Zhang, H. Zhang, K. Zhang, K. Zhang, X. Zhang, X. Zhang, X. Zhang, Z. Zhang, S. Zhao, M. Zhen, B. Zhong, J. Zhu, and X.-F. Zhu, “The ninth visual object tracking vot2021 challenge results,” in *2021 IEEE/CVF International Conference on Computer Vision Workshops (ICCVW)*, pp. 2711–2738, 2021.
- [33] H. K. Galoogahi, A. Fagg, C. Huang, D. Ramanan, and S. Lucey, “Need for Speed: A Benchmark for Higher Frame Rate Object Tracking,” in *2017 IEEE International Conference on Computer Vision (ICCV)*, (Venice), pp. 1134–1143, IEEE, Oct. 2017.
- [34] M. Mueller, N. Smith, and B. Ghanem, “A benchmark and simulator for uav tracking,” in *Computer Vision – ECCV 2016* (B. Leibe, J. Matas, N. Sebe, and M. Welling, eds.), (Cham), pp. 445–461, Springer International Publishing, 2016.
- [35] P. Zhang, J. Zhao, D. Wang, H. Lu, and X. Ruan, “Visible-thermal uav tracking: A large-scale benchmark and new baseline,” in *2022 IEEE/CVF Conference on Computer Vision and Pattern Recognition (CVPR)*, pp. 8876–8885, 2022.
- [36] A. Borne, C. Hennequin, S. Bazeille, P. D. Faria, F. Quint, S. Changey, and C. Cudel, “Military aerial multimodal dataset for RGB-T object tracking: benchmark and efficient algorithm,” in *Autonomous Systems for Security and Defence II* (L. Kampmeijer, B. Masini, and Z. Milosevic, eds.), vol. 13680, p. 136800G, International Society for Optics and Photonics, SPIE, 2025.
- [37] P. Carr and R. T. Collins, “Assessing tracking performance in complex scenarios using mean time between failures,” in *2016 IEEE Winter Conference on Applications of Computer Vision (WACV)*, pp. 1–10, 2016.
- [38] G. Nebehay, *A Deformable Part Model for One-Shot Object Tracking*. PhD thesis, Graz University of Technology, 2016.